Transfer-matrix approach for finite-difference time-domain simulation of periodic structures

Alexei Deinega
Department of Chemistry, Northwestern University, 2145 Sheridan Road, Evanston, Illinois 60208-3113, USA

Sergei Belousov
NRC "Kurchatov Institute", 1 Kurchatov Sq., Moscow, Russia 123182 and Kintech Lab Ltd., 1 Kurchatov Sq., Moscow, Russia 123182

Ilya Valuev
Joint Institute for High Temperatures of RAS, Izhorskaya, 13, build. 2, Moscow, Russia 125412
and Kintech Lab Ltd., 1 Kurchatov Sq., Moscow, Russia 123182

(Received 1 August 2013; published 8 November 2013)

Optical properties of periodic structures can be calculated using the transfer-matrix approach, which establishes a relation between amplitudes of the wave incident on a structure with transmitted or reflected waves. The transfer matrix can be used to obtain transmittance and reflectance spectra of finite periodic structures as well as eigenmodes of infinite structures. Traditionally, calculation of the transfer matrix is performed in the frequency domain and involves linear algebra. In this work, we present a technique for calculation of the transfer matrix using the finite-difference time-domain (FDTD) method and show the way of its implementation in FDTD code. To illustrate the performance of our technique we calculate the transmittance spectra for opal photonic crystal slabs consisting of multiple layers of spherical scatterers. Our technique can be used for photonic band structure calculations. It can also be combined with existing FDTD methods for the analysis of periodic structures at an oblique incidence, as well as for modeling point sources in a periodic environment.

DOI: 10.1103/PhysRevE.88.053305 PACS number(s): 02.60.Cb, 02.70.Bf, 42.70.Qs, 95.75.Pq

I. INTRODUCTION

Photonic crystals (PCs) are artificial structures characterized by periodical variation of the refractive index in space on the length scale comparable to the wavelength of light [1–3]. Owing to the periodicity, the optical properties of PCs are different from the properties of their constituent elements. A wide range of both theoretical and numerical methods has been developed over the years for studying the properties of PCs [4].

Among the methods, the transfer-matrix (T-matrix) technique is widely used for calculation of transmission and reflection coefficients for finite multilayered PC slabs, as well as band structure calculation for the infinite PCs. The term transfer matrix was first introduced by Pendry and MacKinnon [5] in relation to PCs. The idea consists in splitting the structure into elementary slices along a specific direction and analyzing the properties of each slice separately. Essentially, the T matrix relates the fields at one side of the slice to the fields at the other. The T matrix for the whole structure is then given by a simple ordered product of the T matrices for each separate slice, and the optical properties of the structure can be obtained from it.

The T matrix for a single slice can be obtained with the so-called real space transfer-matrix technique, in which the space is divided into a set of small rectangular cells with coupling between neighboring cells [5–8]. In principle, arbitrary structures can be modeled with this method, while the highest efficiency is achieved with periodic structures.

While the T-matrix method can be used to calculate optical properties of structures containing several layers, it proved to be numerically unstable for the thick structures, which should be decomposed into a large number of layers [9]. The instability is caused by multiplication of exponentially growing and decaying terms involved in the T matrix for each separate slice. The problem is solved by using the scattering T matrix in the reciprocal space in the plane of a slice. Such a T matrix can be calculated using the plane-wave transfer-matrix method [10,11]. This method assumes perfectly periodic structure in a slice, which acts as a diffraction grating for the incident light, scattering (reflecting and transmitting) it into a set of directions (diffraction orders). The T matrix relates incident and scattered waves on the left of the slice to the scattered waves on the right of the slice and contains only decaying terms, which guarantees the stability of the method [10–12]. In the scattering T-matrix framework, the slices cannot be simply combined by matrix multiplication, and the calculation of the T matrix for the entire structure can be done via a number of recursive algorithms [9].

In the plane-wave transfer-matrix method, the fields are expanded into the plane-wave series, and T-matrix calculation involves the Fourier transform of both dielectric permittivity of the structure $\epsilon(r)$ and its inverse $\epsilon^{-1}(r)$. This approach becomes inefficient for complex geometries. On-shell layer multiple scattering (LMS) methods [13–15] make use of the symmetry properties of individual objects, constituting the PC layer. At the first step, the T matrix of the object is calculated and then it is used for the calculation of the T matrix of the PC layer. LMS methods are useful when the PC is made of highly symmetrical particles [e.g., spherical in three dimensions (3D) or cylindrical in 2D] [13]. The stacking disorder is naturally incorporated in this approach by application of the proper phase shifts when combining the matrices of adjacent slices [16]. The method can be enhanced to treat spheroids and disk-shaped scatterers [17] but treatment of a generic nonsymmetrical case is complicated.

The finite-difference time-domain method (FDTD) [18] is one of the most powerful methods in computational

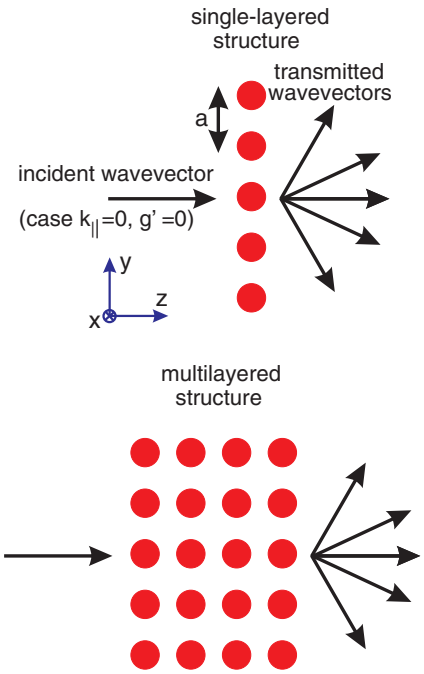

FIG. 1. (Color online) Single-layered (top) or multilayered (bottom) periodic structure (single layer is a periodic array of spheres). Light propagation through these structures can be calculated using the transfer-matrix approach. The transfer matrix of a multilayered structure can be obtained as a product of the transfer matrices of constituent layers.

electrodynamics. In the FDTD framework, the temporal Maxwell's equations are solved on the space-time grid, which makes this method particularly suitable for modeling the structures with an arbitrary geometrical features. The FDTD can be used for calculation of transmittance, reflectance and absorption of finite PC slabs [19], light extraction from OLEDs [20], as well as for spontaneous emission modification modeling [21].

In our previous letter [22] we introduced a new method for calculation of the T matrix for multilayered periodic structures. This method inherits all advantages of the FDTD: it is suitable for simulation of complex geometries and dispersive or nonisotropic media. In our method we perform a series of numerical experiments for a single layer with incident plane-wave impulses of different polarizations and incident wave vectors. Transfer-matrix elements of a single layer are obtained using Fourier transformation of field values recorded during these numerical experiments. The transfer matrix of a multilayered structure can be obtained as a product of T matrices of constituent single layers (Fig. 1). Compared with the direct FDTD simulation of the whole multilayered structure, our approach has an obvious advantage when one needs to vary the number of layers and their positions.

In this paper we present the detailed description of our hybrid FDTD transfer-matrix method and discuss its possible applications. In Sec. II, we outline the scattering T-matrix formulation. In Sec. III, we describe the proposed hybrid method and the way of its implementation in FDTD code. In Sec. IV, we compare our method to both FDTD and the on-shell LMS method for the selected test case. In Sec. V, we discuss further possible developments of our method. In the final Sec. VI, we summarize our results.

II. SCATTERING T-MATRIX FORMULATION

Consider a single-layered planar periodic structure specified by $\mathbf{a_1}$, $\mathbf{a_2}$ primitive vectors in the in xy plane (Fig. 1, top). The corresponding reciprocal-lattice primitive vectors $\mathbf{b}_1$, $\mathbf{b}_2$ satisfy the relation

$$\mathbf{b}_i \cdot \mathbf{a}_j = 2\pi\delta_{ij}. \tag{1}$$

For a single plane wave the wave vector $\mathbf{q}$ can be represented as a sum of components parallel and normal to the layer:

$$\mathbf{q} = \mathbf{q}_\parallel + \mathbf{q}_z. \tag{2}$$

One can write the component parallel to the layer as

$$\mathbf{q}_\parallel = \mathbf{k}_\parallel + \mathbf{g}, \tag{3}$$

where $\mathbf{k}_\parallel$ belongs to the first surface Brillouin zone formed by vectors $\mathbf{b}_1$, $\mathbf{b}_2$ and $\mathbf{g}$ is translation vector in reciprocal space, $\mathbf{g} = m_1\mathbf{b}_1 + m_2\mathbf{b}_2$.

Let us consider some fixed value $\mathbf{k}_\parallel$. The wave vector of the plane wave with some given frequency ω and $\mathbf{q}_\parallel = \mathbf{k}_\parallel + \mathbf{g}$ can be written as:

$$\mathbf{q}_\mathbf{g}^\pm = \mathbf{k}_\parallel + \mathbf{g} \pm [q^2 - (\mathbf{k}_\parallel + \mathbf{g})^2]^{\frac{1}{2}}\mathbf{u}_z, \tag{4}$$

where $+$ and $-$ signs correspond to wave propagating in the positive and negative z direction respectively, $\mathbf{u}_z$ is the unit vector in the positive z direction, and $q^2 = \mu\epsilon(\omega/c)^2$. In the case $q^2 < (\mathbf{k}_\parallel + \mathbf{g})^2$, (4) defines a wave decaying in the positive or negative z direction.

Plane waves $\exp(i\mathbf{q}_\mathbf{g}^s \cdot \mathbf{r})\mathbf{u}_j$ with a given $\mathbf{g}$, direction $s = \pm$, polarization $j = 1,2$, and vector $\mathbf{g}$ may be used as a basis for the electric (magnetic) field characterized by fixed frequency ω and $\mathbf{k}_\parallel$:

$$\mathbf{E}(\mathbf{r}) = \sum_{s=\pm}\sum_{j=1}^{2}\sum_{\mathbf{g}}[E]^s_{\mathbf{g}j}\exp\left(i\mathbf{q}_\mathbf{g}^s \cdot \mathbf{r}\right)\mathbf{u}_j. \tag{5}$$

We agree that $j = 1$ corresponds to the s-polarized wave, whereas $j = 2$ corresponds to the p-polarized wave, and $\mathbf{u}'_j$ is a unit vector in a direction of polarization. Obviously, vector $\mathbf{u}_j$ is perpendicular to the incident wave vector $\mathbf{q}_\mathbf{g}^+$. For the special case when $\mathbf{q}_\mathbf{g}^+$ is directed along the z direction (normal incidence), we make an agreement that $j = 1,2$ correspond to x and y axes, respectively.

Let the incident field propagate in the positive z direction. Then its expansion takes the form

$$\mathbf{E}^+_{\text{in}}(\mathbf{r}) = \sum_{j'=1}^{2}[E_{\text{in}}]^+_{\mathbf{g}'j'}\exp(i\mathbf{q}^+_{\mathbf{g}'} \cdot \mathbf{r})\mathbf{u}_{j'}, \tag{6}$$

where $[E_{\text{in}}]^{s'}_{\mathbf{g}'j'}$ are expansion coefficients. Here and after we use the strokes $'$ to mark the incident wave, while the absence of stroke can refer to transmitted or reflected waves.

Generally, the transmitted and reflected fields may be represented as:

$$\mathbf{E}^{+}_{\mathrm{tr}}(\mathbf{r}) = \sum_{j=1}^{2}\sum_{\mathbf{g}}[E_{\mathrm{tr}}]^{+}_{\mathbf{g}j}\exp(i\mathbf{q}^{+}_{\mathbf{g}}\cdot\mathbf{r})\mathbf{u}_j, \tag{7}$$

$$\mathbf{E}^{-}_{\mathrm{rf}}(\mathbf{r}) = \sum_{j=1}^{2}\sum_{\mathbf{g}}[E_{\mathrm{rf}}]^{-}_{\mathbf{g}j}\exp(i\mathbf{q}^{-}_{\mathbf{g}}\cdot\mathbf{r})\mathbf{u}_j. \tag{8}$$

The $+$ sign for the transmitted wave in (7) means that it propagates in the positive z direction. The $-$ sign for the reflected wave (8) means that it propagates in the negative z direction. Due to the translational symmetry of the structure, the part $\mathbf{k}_{\parallel}$ of the planar wave vector $\mathbf{q}_{\parallel}$ (which belongs to the first Brillouin zone) remains the same for the incident (6), transmitted (7) and reflected (8) waves.

While these expansions in principle include the infinite series over $\mathbf{g}$, in numerical applications there is always a cutoff at some value and the sum is finite: $|\mathbf{g}| \leqslant g_{\max}$. The cutoff value $g_{\max}$ should be chosen so as to guarantee the convergence of the reflected and transmitted fields. One can choose $g_{\max} = \mu\varepsilon(\omega_{\max}/c)^2$ where $\omega_{\max}$ is a maximal calculated frequency. In this case directions $|\mathbf{g}| > g_{\max}$ will correspond to evanescent waves only.

Because of the linearity of Maxwell's equations, passage of the plane wave of given frequency (given q) through the periodic structure can be regarded as an action of a linear operator in the space of indices $\{m_1, m_2\}$ and two polarizations. Therefore the expansion coefficients $[E_{\mathrm{tr}}]^{+}_{\mathbf{g}i}$ for the transmitted and $[E_{\mathrm{rf}}]^{-}_{\mathbf{g}i}$ for reflected waves, entering the relations (7) and (8), can be expressed through the expansion coefficients $[E_{\mathrm{in}}]^{+}_{\mathbf{g}'j'}$ for the incident wave (6). This can be done by introducing transmission $M^{++}_{\mathbf{g}i,\mathbf{g}'j'}$ and reflection $M^{-+}_{\mathbf{g}i,\mathbf{g}'j'}$ matrix elements:

$$[E_{\mathrm{tr}}]^{+}_{\mathbf{g}j} = \sum_{j'=1}^{2} M^{++}_{\mathbf{g}j,\mathbf{g}'j'}[E_{\mathrm{in}}]^{+}_{\mathbf{g}'j'}, \tag{9}$$

$$[E_{\mathrm{rf}}]^{-}_{\mathbf{g}j} = \sum_{j'=1}^{2} M^{-+}_{\mathbf{g}j,\mathbf{g}'j'}[E_{\mathrm{in}}]^{+}_{\mathbf{g}'j'}. \tag{10}$$

Now assume that the incident plane wave propagates in the negative z direction:

$$\mathbf{E}^{-}_{\mathrm{in}}(\mathbf{r}) = \sum_{j'=1}^{2}[E_{\mathrm{in}}]^{-}_{\mathbf{g}'j'}\exp(i\mathbf{q}^{-}_{\mathbf{g}'}\cdot\mathbf{r})\mathbf{u}'_j. \tag{11}$$

The transmission and reflection matrix elements $M^{--}_{\mathbf{g}i,\mathbf{g}'j'}$, $M^{+-}_{\mathbf{g}i,\mathbf{g}'j'}$ are defined in the similar way:

$$[E_{\mathrm{tr}}]^{-}_{\mathbf{g}j} = \sum_{j'=1}^{2} M^{--}_{\mathbf{g}j,\mathbf{g}'j'}[E_{\mathrm{in}}]^{-}_{\mathbf{g}'j'} \tag{12}$$

$$[E_{\mathrm{rf}}]^{+}_{\mathbf{g}j} = \sum_{j'=1}^{2} M^{+-}_{\mathbf{g}j,\mathbf{g}'j'}[E_{\mathrm{in}}]^{-}_{\mathbf{g}'j'}. \tag{13}$$

The action of $M^{\pm,\pm}$ on the incident wave $[E_{\mathrm{in}}]^{\pm}$ in (9), (10), (12), (13) can be thought of as *transferring* it to the transmitted (reflected) wave on the other (the same) side of the layer. This is graphically represented in Fig. 2.

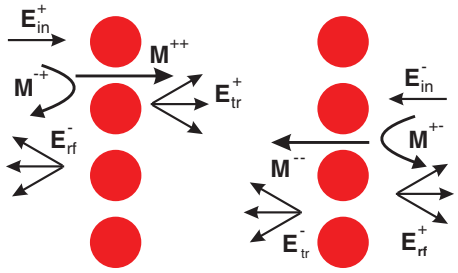

FIG. 2. (Color online) Scattering of the incident wave on the single layer of periodic structure: the action of M matrices.

Let us now consider a multilayered structure (Fig. 1, bottom). The transmission and reflection matrices for the structure can be obtained from the matrices for each layer. Each layer can be characterized by the left ($-\mathbf{d}_l$) and right ($\mathbf{d}_r$) virtual borders with respect to its center $z = 0$ (Fig. 3). Expressing the plane waves to the left (right) of the layer with respect to its left (right) border (i.e., a plane wave to the left of the layer reads $\mathbf{E}^{\pm}_{\mathbf{g}}\exp[i\mathbf{q}^{\pm}_{\mathbf{g}}(\mathbf{r}+\mathbf{d}_l)]$, and the plane wave to the right $\mathbf{E}^{\pm}_{\mathbf{g}}\exp[i\mathbf{q}^{\pm}_{\mathbf{g}}(\mathbf{r}-\mathbf{d}_r)]$) we can rewrite the matrices M in the following form:

$$Q^{\mathrm{I}}_{\mathbf{g}j,\mathbf{g}'j'} = M^{++}_{\mathbf{g}j,\mathbf{g}'j'}\exp[i\mathbf{q}^{+}_{\mathbf{g}}\cdot\mathbf{d}_r + i\mathbf{q}^{+}_{\mathbf{g}'}\cdot\mathbf{d}_l], \tag{14}$$

$$Q^{\mathrm{II}}_{\mathbf{g}j,\mathbf{g}'j'} = M^{+-}_{\mathbf{g}j,\mathbf{g}'j'}\exp[i\mathbf{q}^{+}_{\mathbf{g}}\cdot\mathbf{d}_r - i\mathbf{q}^{-}_{\mathbf{g}'}\cdot\mathbf{d}_r], \tag{15}$$

$$Q^{\mathrm{III}}_{\mathbf{g}j,\mathbf{g}'j'} = M^{-+}_{\mathbf{g}j,\mathbf{g}'j'}\exp[-i\mathbf{q}^{-}_{\mathbf{g}}\cdot\mathbf{d}_l + i\mathbf{q}^{+}_{\mathbf{g}'}\cdot\mathbf{d}_l], \tag{16}$$

$$Q^{\mathrm{IV}}_{\mathbf{g}j,\mathbf{g}'j'} = M^{--}_{\mathbf{g}j,\mathbf{g}'j'}\exp[-i\mathbf{q}^{-}_{\mathbf{g}}\cdot\mathbf{d}_l - i\mathbf{q}^{-}_{\mathbf{g}'}\cdot\mathbf{d}_r]. \tag{17}$$

Matrices Q^{I} and Q^{III} correspond to the incident wave propagating in the positive z direction: matrix Q^{I} relates the transmitted wave (with respect to the right border) to the incident wave (with respect to the left border), matrix Q^{III} relates the reflected wave (with respect to the left border) to the incident wave (with respect to the left border). Matrices Q^{II} and Q^{IV} correspond to the incident wave propagating in the negative z direction and have the similar meaning.

Once the Q matrices for two adjacent layers (n and $n+1$) are obtained, Q matrices for the pair of them can be calculated. Let a plane wave $\mathbf{E}^{+}_{\mathrm{in}}$ be once again incident from the left on the pair of layers. We denote the reflected wave as $\mathbf{E}^{-}_{\mathrm{rf}}$, and the transmitted wave as $\mathbf{E}^{+}_{\mathrm{tr}}$, while the wave propagating in the positive (negative) direction in between the adjacent layers is

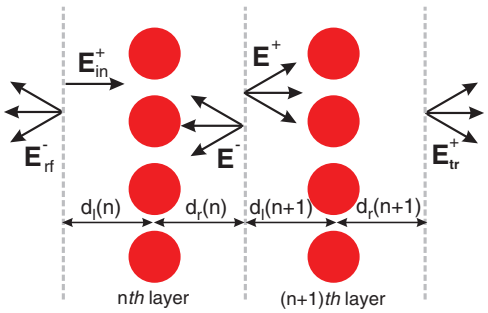

FIG. 3. (Color online) Scattering of the incident wave on the pair of layers: setting up the virtual borders $\mathbf{d}_{l,r}$.

denoted as $\mathbf{E}^+$ ($\mathbf{E}^-$), see Fig. 3. Using Q matrices we obtain

$$\mathbf{E}^+ = Q^{\mathrm{I}}(n)\mathbf{E}^+_{\mathrm{in}} + Q^{\mathrm{II}}(n)\mathbf{E}^-, \tag{18}$$

$$\mathbf{E}^- = Q^{\mathrm{III}}(n+1)\mathbf{E}^+, \tag{19}$$

and therefore

$$\mathbf{E}^+ = [I - Q^{\mathrm{II}}(n)Q^{\mathrm{III}}(n+1)]^{-1}Q^{\mathrm{I}}(n)\mathbf{E}^+_{\mathrm{in}}, \tag{20}$$

where I is unity matrix.

Then, for the transmitted and reflected waves we arrive at the following relations

$$\mathbf{E}^+_{\mathrm{tr}} = Q^{\mathrm{I}}(n+1)[I - Q^{\mathrm{II}}(n)Q^{\mathrm{III}}(n+1)]^{-1}Q^{\mathrm{I}}(n)\mathbf{E}^+_{\mathrm{in}}, \tag{21}$$

$$\mathbf{E}^-_{\mathrm{rf}} = \{Q^{\mathrm{III}}(n) + Q^{\mathrm{IV}}(n)Q^{\mathrm{III}}(n+1) \times [I - Q^{\mathrm{II}}(n)Q^{\mathrm{III}}(n+1)]^{-1}Q^{\mathrm{I}}(n)\}\mathbf{E}^+_{\mathrm{in}}. \tag{22}$$

Comparing the above equations to the definitions of corresponding Q matrices, we finally obtain the Q matrices for of a pair of adjacent layers $n, n+1$:

$$Q^{\mathrm{I}}(n,n+1) = Q^{\mathrm{I}}(n+1) \times [I - Q^{\mathrm{II}}(n)Q^{\mathrm{III}}(n+1)]^{-1}Q^{\mathrm{I}}(n), \tag{23}$$

$$Q^{\mathrm{III}}(n,n+1) = Q^{\mathrm{III}}(n) + Q^{\mathrm{IV}}(n)Q^{\mathrm{III}}(n+1) \times [I - Q^{\mathrm{II}}(n)Q^{\mathrm{III}}(n+1)]^{-1}Q^{\mathrm{I}}(n). \tag{24}$$

Identical considerations for a plane wave incident on the pair of layers from the right lead to similar expressions for $Q^{\mathrm{IV}}(n,n+1)$ and $Q^{\mathrm{II}}(n,n+1)$ correspondingly. The described procedure of multiplying the Q matrices of a pair of adjacent layers can be repeated until one gets the Q matrices for the whole multilayered structure.

Q matrices can be used to obtain transmission and reflection coefficients for the multilayered structure. Assuming that the incident wave propagates in the positive z direction, the transmitted and reflected waves for the whole structure can be written similarly to (9), (10):

$$[E_{\mathrm{tr}}]^+_{\mathbf{g}j} = \sum_{j'=1}^{2} Q^{\mathrm{I}}_{\mathbf{g}j,\mathbf{g}'j'}[E_{\mathrm{in}}]^+_{\mathbf{g}'j'}, \tag{25}$$

$$[E_{\mathrm{rf}}]^-_{\mathbf{g}j} = \sum_{j'=1}^{2} Q^{\mathrm{III}}_{\mathbf{g}j,\mathbf{g}'j'}[E_{\mathrm{in}}]^+_{\mathbf{g}'j'}. \tag{26}$$

Summing intensities of the transmitted (25) and reflected (26) waves over $\mathbf{g}$ and j and normalizing by the incident wave intensity, we find the transmission and reflection coefficients for the incident wave (6):

$$T = \frac{\sum_{\mathbf{g},j} |[E_{\mathrm{tr}}]^+_{\mathbf{g}j}|^2 q^+_{\mathbf{g}z}}{\sum_{j'} |[E_{\mathrm{in}}]^+_{\mathbf{g}'j'}|^2 q^+_{\mathbf{g}'z}}, \tag{27}$$

$$R = \frac{\sum_{\mathbf{g},j} |[E_{\mathrm{rf}}]^-_{\mathbf{g}j}|^2 q^+_{\mathbf{g}z}}{\sum_{j'} |[E_{\mathrm{in}}]^+_{\mathbf{g}'j'}|^2 q^+_{\mathbf{g}'z}}, \tag{28}$$

where $q^+_{\mathbf{g}z} = [q^2 - (\mathbf{k}_\parallel + \mathbf{g})^2]^{\frac{1}{2}}$ and $q^+_{\mathbf{g}'z} = [q^2 - (\mathbf{k}_\parallel + \mathbf{g}')^2]^{\frac{1}{2}}$, compare with (4).

Q matrices can be used to calculate the band structure of infinite PCs. An infinite PC can be represented as a block of (generally) several layers repeating infinitely along the z axis. The complex band structure associated with the xy surface of the PC can be obtained by applying the Bloch periodic boundary conditions along z and taking into account the relation between the fields immediately to the left and to the right of the block via the corresponding Q matrices [11,14,15]. Varying the phase in the Bloch periodic boundary conditions along z direction, one can obtain the band structure in the whole reciprocal space.

III. HYBRID METHOD

In this section we describe a way of calculating the M matrix elements (9), (10), (12), (13) using the FDTD method. Since we consider a periodic structure, a single unit cell with the periodic boundary conditions may be simulated. Generally, the FDTD method allows us to specify either periodic ($\mathbf{k}_\parallel = 0$) or Bloch-periodic boundary conditions of the form:

$$\mathbf{F}(t,\mathbf{r}) = \mathbf{F}(t,\mathbf{r} \pm \mathbf{a}) \exp(\pm i\mathbf{k}_\parallel \cdot \mathbf{a}), \tag{29}$$

where $\mathbf{F}$ is either electric field $\mathbf{E}$ or magnetic field $\mathbf{H}$, $\mathbf{a}$ is a lattice translation vector parallel to the surface of the structure, t and $\mathbf{r}$ are the coordinates in time and space.

For simplicity, in this section we consider the case of $\mathbf{k}_\parallel = 0$ (extension for nonzero $\mathbf{k}_\parallel$ is trivial). In this case, every possible transmission and reflection directions correspond to the wave vectors of the form

$$\mathbf{q} = \mathbf{g} + \mathbf{q}_z, \tag{30}$$

where $\mathbf{g} = m_1\mathbf{b}_1 + m_2\mathbf{b}_2$ and $\mathbf{b}_1$, $\mathbf{b}_2$ are the elementary translations in the reciprocal lattice. Note that any periodical structure can be considered for the only case $\mathbf{k}_\parallel = 0$ when using the multiple elementary cells (supercell) in the xy plane. The supercell approach is however very extensive in terms of computational resources. An alternative is the application of the Bloch-periodic boundary conditions defined for each specific value of $\mathbf{k}_\parallel$. The calculation procedure for the matrix elements for each $\mathbf{k}_\parallel$ remains the same as described below for the periodic case but requires FDTD implementation with the Bloch-periodic boundary conditions.

Our FDTD geometry setup is illustrated at Fig. 4, where the structure is periodic in the x and y directions, and finite in the z direction. Nonperiodical directions are confined by the perfectly matched layers (PMLs) [18]. To generate the incident wave we use the total field/scattered field (TF/SF) technique [18].

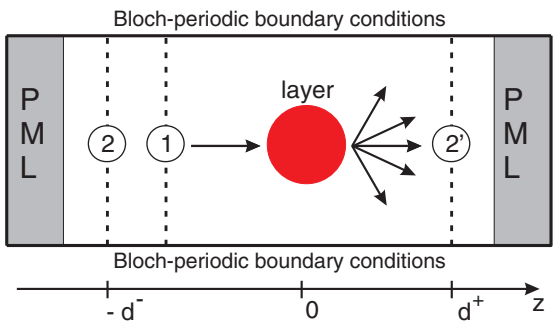

FIG. 4. (Color online) FDTD geometry setup. 1: generating (TF/SF) border; 2, 2′: detector arrays for reflected and transmitted waves.

The TF/SF surface positioned before the structure interface generates an electromagnetic pulse propagating along the z direction. The pulse signal is partially reflected from the structure and is absorbed into the rear PMLs layer. The rest of the pulse propagates through the structure and is absorbed into the fore PMLs layer. The FDTD simulation runs until the signal has left the computational cell. The simulation time depends on the geometry as well as optical properties of the simulated structure. Usually, the greater the length of the structure is in the z direction, the longer is the duration of the experiment, as the path covered by the signal before leaving the structure increases. Also, the duration is usually shorter for absorbing structures as compared to purely dielectric ones.

The incident pulse is a wave packet with a temporal profile $g(t)$ chosen in such a way as to cover the desired frequency range. Using a pulse with finite duration allows to obtain results for a wide frequency range per one simulation. For example, temporal profile of the pulse can be defined by Gaussian centered at some time $t = t_0$

$$g(t) = \exp\left[-\left(\frac{t-t_0}{t_w}\right)^2\right], \tag{31}$$

which has the following frequency representation

$$g(\omega) = t_w \pi^{1/2} \exp\left[-\frac{\omega^2 t_w^2}{4}\right]. \tag{32}$$

Changing t_w one can tune frequency range covered by the pulse. Frequencies covered by the pulse should be resolved by FDTD mesh (standard Yee mesh resolves wavelengths not less than 10–20 mesh steps [18]). Note that the temporal profile of the Gaussian pulse (31) has a nonzero value at $t = 0$. To provide a smooth transition from zero into Gaussian pulse we should have at least $t_0 > 3t_w$. We also need to terminate the Gaussian pulse after some time t_e:

$$g(t) = 0, \quad t > t_e, \tag{33}$$

which should be at least $t_e > t_0 + 3t_w$.

To apply the TF/SF technique one needs to know the incident field at the mesh nodes closest to the TF/SF surface. For the normal incidence, $\mathbf{g} = 0$, the incident field is given by:

$$\mathbf{E}(t,\mathbf{r}) = g(t - z/c)\mathbf{u}_j, \tag{34}$$

where $\mathbf{u}_j$ is the chosen polarization vector. One can use the expression (34) to specify the incident field in the TF/SF technique. However, it does not perfectly reproduce the actual numerical incident pulse propagation in the FDTD mesh. To deal with this problem, instead of using analytical expression (34), one can calculate the incident field at an auxiliary one-dimensional grid [18].

If the incident wave has a nonzero component $\mathbf{g} \neq 0$, then the wave vector depends on the frequency as

$$\mathbf{q}(\omega) = \mathbf{g} + \sqrt{\mu\varepsilon(\omega/c)^2 - \mathbf{g}^2}\,\mathbf{u}_z, \tag{35}$$

where $\mathbf{u}_z$ is a unit vector in z direction. The expression (35) is a special case of (4) with $\mathbf{k}_\parallel = 0$. To model the finite pulse one can choose the frequency representation of some known pulse $g(\omega)$:

$$\mathbf{E}(\mathbf{r},\omega) = g(\omega)\mathbf{u}_j e^{i\mathbf{qr}} = g(\omega)\mathbf{u}_j e^{iz\sqrt{\mu\epsilon(\omega/c)^2 - \mathbf{g}^2}} e^{i\mathbf{gr}}. \tag{36}$$

The resulting pulse in the time domain can be obtained as

$$\begin{aligned}\mathbf{E}(\mathbf{r},t) &= \mathrm{Re}(\hat{\mathbf{F}}_\omega[g(\omega)\mathbf{u}_j e^{i\mathbf{qr}}]) \\ &= \mathrm{Re}(\hat{\mathbf{F}}_\omega[g(\omega)\mathbf{u}_j e^{iz\sqrt{\mu\epsilon(\omega/c)^2 - \mathbf{g}^2}}]e^{i\mathbf{gr}}),\end{aligned} \tag{37}$$

where $\hat{\mathbf{F}}_\omega$ denotes the inverse Fourier transform. The same form of the incident pulse is used in the spectral FDTD method [23]. Note that the resulting pulse (37) should be terminated after some time (33) when it is small enough.

Expressions (34) and (37) can be applied for magnetic field $\mathbf{H}$ as well. If the incident medium has a refractive index different from unity, then (34), (37) should be be multiplied on it while applying for magnetic field.

S- and p-polarization directions can be defined as: $\mathbf{u}_s = (\mathbf{q} \times \mathbf{u}_z)/|\mathbf{q} \times \mathbf{u}_z|$, $\mathbf{u}_p = \mathbf{q} \times \mathbf{u}_s$. Note that the incident pulse (37) includes evanescent components $\mu\epsilon(\omega/c)^2 < \mathbf{g}^2$ with a complex vector $\mathbf{q}$, which has its imaginary part along the z direction. In this case, $\mathbf{u}_p = \mathbf{q} \times \mathbf{u}_s$ is a complex vector as well. However, the vector $\mathbf{u}_s$ is always real, since $\mathbf{q} \times \mathbf{u}_z$ is also real ($\mathbf{q}$ does not have imaginary components in the xy plane).

For the case $\mathbf{g} \neq 0$, different plane waves components of the pulse propagate along different directions. Therefore we cannot use only one auxiliary one-dimensional grid to calculate the incident wave propagation. Propagation of different components can be calculated at separate One-dimensional meshes, but it is easier to use directly the analytical form of the incident pulse (37). However, as we found numerically, in this case TF/SF surface can generate certain artificial evanescent waves in backward direction.

To calculate the transmitted and reflected waves $\mathbf{E}(\omega,\mathbf{g})$ we put planar detector arrays in front of (for transmitted wave) and behind (for reflected wave) the structure. The detectors do not correspond to real objects in space. We use the term detector to denote the points where field values are recorded. Note that these points do not necessarily coincide with the FDTD mesh nodes. They could be positioned arbitrarily inside calculated volume. Field values at the detectors are interpolated by mesh. Our detectors are arranged in a two-dimensional xy grid with spatial steps Δx, Δy.

During the numerical experiment the detectors record field $\mathbf{E}(t,x,y)$ in time and space representation (z coordinate is fixed since the detectors plane is perpendicular to z direction). Field values $\mathbf{E}(\omega,g_x,g_y)$ can be obtained using Fourier transformations in time $t \to \omega$ and space $x,y \to g_x,g_y$. Order of these Fourier transformations is irrelevant: one can make the temporal Fourier transformation first, and the spatial Fourier transformation after (and vice versa).

The Fourier transformation $t \to \omega$ can be done using the Fourier-on-the-fly procedure, which assumes a separate subsuming of the Fourier transformation for each frequency ω at each temporal iteration n:

$$\mathbf{E}(\omega) = \sum_{n=0}^{N_t} \mathbf{E}(t)\exp(i\omega n\Delta t)\Delta t, \tag{38}$$

where Δt is the time step and N_t is the number of temporal iterations. However, if one needs to obtain the fields in a wide frequency range, it is more efficient to record the time history of a signal and perform the fast Fourier transformation [24]

at the end of the simulation. The drawback of this approach is necessity to keep the whole time trace of the signal in the computer memory. If the simulation is long it leads to allocating huge arrays in the memory for the recorded field values. As an alternative, field values can be recorded in some file at the each temporal iteration. This file will be analyzed at the end of the simulation.

The spatial Fourier transformation $x,y \to g_x,g_y$ should be done using the Fourier-on-the-fly method, since the number of wave vectors of interest is usually small. In the case of parallel FDTD implementation, each processor can calculate a partial subsum of the Fourier transform for detectors inside the corresponding space subdomain. At the end of the calculation all partial subsums are collected at a chosen processor and the total sum is calculated:

$$\mathbf{E}(g_x,g_y) = \sum_{k=0}^{N_x}\sum_{l=0}^{N_y}\mathbf{E}(x,y)\exp\left(\mathrm{i}g_x k\Delta x + \mathrm{i}g_y l\Delta y\right)\Delta x\Delta y, \tag{39}$$

where Δx, Δy are the spacings of detectors array, and N_x, N_y are the dimensions of detectors array in corresponding directions.

Let us roughly estimate the number of operations for two different ways of Fourier transformation: $\mathbf{E}(t,x,y) \to \mathbf{E}(t,g_x,g_y) \to \mathbf{E}(\omega,g_x,g_y)$ and $\mathbf{E}(t,x,y) \to \mathbf{E}(\omega,x,y) \to \mathbf{E}(\omega,g_x,g_y)$. We use the following notations: N_t is the number of the temporal iterations, $N_r = N_x N_y$ is the number of detectors, N_ω is the number of calculated frequencies, N_g is the number of calculated components $\mathbf{g}$. Calculating sum (38) for all frequencies consumes $N_t N_\omega$ operations. Calculating sum (39) for all components $\mathbf{g}$ consumes $N_r N_g$ operations. Performing the temporal Fourier transformation (for all components $\mathbf{g}$) after the spatial Fourier transformation (for all time iterations) consumes $N_g N_t N_\omega + N_t N_r N_g$ operations. Performing the temporal Fourier transformation (for all detectors) before the spatial Fourier transformation (for all frequencies) consumes $N_\omega N_r N_g + N_r N_t N_\omega$ operations. Since the number of detectors is usually larger then the number of time steps $N_r \geqslant N_t$ (detectors are arranged in a *two*-dimensional array in the xy plane, while time is *one*-dimensional), the first way is more efficient since it requires less operations. However, if one needs to calculate $E(\omega,x,y)$, the second way should be chosen. For example, the frequency-dependent field $E(\omega,x,y)$ can be used to analyze spatial distribution of different modes (in frequency domain) or calculate transmitted (reflected) flux spectra:

$$W(\omega) = \frac{1}{2}\int \mathrm{Re}\,|\mathbf{E}(\omega,x,y)^* \times \mathbf{H}(\omega,x,y)| \cdot \mathbf{u}_z dS, \tag{40}$$

where the integration is performed through the area S covered by the detector arrays for the transmitted (reflected) waves. Note that the energy flux can also be calculated as a sum over the propagating waves fluxes:

$$W(\omega) = \frac{1}{2}\sum_{q_z{}^2>0}\mathrm{Re}\,|\mathbf{E}(\omega,g_x,g_y)^* \times \mathbf{H}(\omega,g_x,g_y)| S\cos\theta, \tag{41}$$

where θ is the propagation angle, $\cos\theta = (\mathbf{q}\cdot\mathbf{u}_z)/|\mathbf{q}|$, $\mathbf{q}$ is the transmitted or reflected wave vector (35).

In our method we simulate the incident light of different components $\mathbf{g}'$ and polarizations j' according to (37). For each pair $(\mathbf{g}',j')$ we make two numerical experiments: with the structure and without the structure (vacuum). We perform the Fourier transformation of the recorded fields $\mathbf{E}(t,x,y) \to \mathbf{E}(\omega,g_x,g_y)$ and calculate their projection onto s- and p-polarization directions $E(\omega,\mathbf{g},j) = \mathbf{E}(\omega,\mathbf{g})\cdot\mathbf{u}_j$, $j = s,p$.

Let us denote the calculated transmitted and reflected fields for the structure and vacuum experiments as $E^+_{\mathrm{str}}(\omega,\mathbf{g},j)$, $E^-_{\mathrm{str}}(\omega,\mathbf{g},j)$, $E^+_{\mathrm{vac}}(\omega,\mathbf{g},j)$, $E^-_{\mathrm{vac}}(\omega,\mathbf{g},j)$. Since the incident wave has a fixed component $\mathbf{g}'$ and polarization j', $E^+_{\mathrm{vac}}(\omega,\mathbf{g},j)$ and $E^-_{\mathrm{vac}}(\omega,\mathbf{g},j)$ should be nonzero only for $\mathbf{g}' = \mathbf{g}$ and $j = j'$. Field $E^-_{\mathrm{vac}}(\omega,\mathbf{g}',j')$ is close to zero for normal incidence case $\mathbf{g}' = 0$ (it is still nonzero due to the small spurious wave propagating backwards from the TF/SF border). However, for the components $\mathbf{g}' \neq 0$ field value $E^-_{\mathrm{vac}}(\omega,\mathbf{g}',j')$ is not small enough to be ignored. As was discussed earlier, the TF/SF border generates the spurious backward wave together with the incident field (37) with nonzero $\mathbf{g}'$.

If the incident wave has a component $\mathbf{g}'$ and polarization j', we have:

$$[E_{\mathrm{tr}}]^+_{\mathbf{g}j} = M^{++}_{\mathbf{g}j,\mathbf{g}'j'}[E_{\mathrm{in}}]^+_{\mathbf{g}'j'}, \tag{42}$$

$$[E_{\mathrm{rf}}]^-_{\mathbf{g}j} = M^{-+}_{\mathbf{g}j,\mathbf{g}'j'}[E_{\mathrm{in}}]^+_{\mathbf{g}'j'}, \tag{43}$$

which is particular case of (9), (10). These relations imply a way how to obtain the transfer matrix elements with the help of FDTD. One needs to simulate incident wave with the fixed component $\mathbf{g}$ and polarization, then find the transmitted and reflected fields and normalize them to the incident field:

$$M^{++}_{\mathbf{g}j,\mathbf{g}'j'} = [E_{\mathrm{tr}}]^+_{\mathbf{g}j}/[E_{\mathrm{in}}]^+_{\mathbf{g}'j'}, \tag{44}$$

$$M^{-+}_{\mathbf{g}j,\mathbf{g}'j'} = [E_{\mathrm{rf}}]^-_{\mathbf{g}j}/[E_{\mathrm{in}}]^+_{\mathbf{g}'j'}. \tag{45}$$

This procedure can be repeated for different incident components $\mathbf{g}'$ and the two possible polarizations.

To calculate the transfer-matrix elements (44), (45) we need to reconstruct the transmitted, reflected, and incident waves at the position $z = 0$. These field values are obtained from the fields recorded by the detectors by applying the corresponding phase shifts (see Fig. 4):

$$[E^+_{\mathrm{in}}]_{\mathbf{g},j} = E^+_{\mathrm{vac}}(\mathbf{g},j)\exp(-id^+\sqrt{\mu\epsilon(\omega/c)^2 - \mathbf{g}^2}), \tag{46}$$

$$[E^+_{\mathrm{tr}}]_{\mathbf{g},j} = E^+_{\mathrm{str}}(\mathbf{g},j)\exp(-id^+\sqrt{\mu\epsilon(\omega/c)^2 - \mathbf{g}^2}), \tag{47}$$

$$[E^-_{\mathrm{rf}}]_{\mathbf{g},j} = (E^-_{\mathrm{str}}(\mathbf{g},j) - E^-_{\mathrm{vac}}(\mathbf{g},j)) \cdot \exp(id^-\sqrt{\mu\epsilon(\omega/c)^2 - \mathbf{g}^2}), \tag{48}$$

where d^+ (d^-) is the distance between transmittance (reflectance) detectors arrays and $z = 0$ position. In the last relation (48) we take into account that the signal recorded by reflectance detectors is partially contributed by the artificial signal generated by the TF/SF surface and propagating backwards. The fields (46)–(48) should be substituted to (44), (45) to calculate the transfer-matrix elements.

If the scatterers constituting adjacent layers are far from each other, the transfer-matrix elements corresponding to

the evanescent waves $\mu\varepsilon(\omega_{\max}/c)^2 > \mathbf{g}^2$ can be neglected, since the evanescent waves centered at these scatterers decay fast with increasing distance and do not reach adjacent layers. If this is not the case, we still need to calculate the transfer-matrix elements for the evanescent components. This procedure requires some precautions described in the next two paragraphs.

As we found numerically, while applying (37) as an incident impulse, the TF/SF surface generates spurious evanescent waves $[E_{\text{in}}]^+_{\mathbf{g}'j'}$ of the opposite component $-\mathbf{g}'$ or conjugate polarization [waves with $\mathbf{g} \neq \pm\mathbf{g}'$ do not appear because of the oscillating coefficient $\exp(i\mathbf{g}'\mathbf{r})$ in (37)]. These spurious waves are smaller than that one with $\mathbf{g}', j'$, but not small enough to be ignored. This makes problematic extracting the transfer matrix elements within one FDTD experiment (44), (45) for frequencies $\mu\varepsilon(\omega/c)^2 > \mathbf{g}^2$. To solve this problem, we combine four numerical experiments with both components $\pm\mathbf{g}'$ and polarizations $j' = s, p$. As a result, we arrive to system of four linear equations for four unknowns $M^{\pm+}_{\mathbf{g}j,\mathbf{g}'j'}$.

$$[E_{\text{tr}}]^+_{\mathbf{g}j} = \sum_{j'=1}^{2} \sum_{\pm\mathbf{g}'} M^{++}_{\mathbf{g}j,\mathbf{g}'j'} [E_{\text{in}}]^+_{\mathbf{g}'j'}, \tag{49}$$

$$[E_{\text{rf}}]^-_{\mathbf{g}j} = \sum_{j'=1}^{2} \sum_{\pm\mathbf{g}'} M^{-+}_{\mathbf{g}j,\mathbf{g}'j'} [E_{\text{in}}]^+_{\mathbf{g}'j'}. \tag{50}$$

Each linear equation contains a different combination of $[E_{\text{in}}]^+_{\mathbf{g}'j'}$ which correspond to the true wave and three spurious waves generated in each experiment. This system is well conditioned and can be easily solved using standard linear algebra.

While modeling the evanescent waves, the TF/SF surface and detectors should be placed close to the structure, since these waves decay fast with the distance but should not be missed. At the same time, the distance between PML and structure should not be small, since the evanescent waves are poorly absorbed by the PML. In some cases, interaction between the PML and evanescent waves can lead to a special kind of the FDTD divergence [25]. To solve this problem one may increase the distance between the PML and the structure, however it involves using larger computational mesh. A better solution is to apply an additional absorbing layer behind the PML [24]. This layer absorbs transverse and evanescent waves, which are problematic for the standard PML.

We described above how to calculate the transfer-matrix elements $M^{++}_{\mathbf{g}j,\mathbf{g}'j'}$, $M^{-+}_{\mathbf{g}j,\mathbf{g}'j'}$. Elements $M^{--}_{\mathbf{g}j,\mathbf{g}'j'}$, $M^{+-}_{\mathbf{g}j,\mathbf{g}'j'}$ are calculated in the same way by simulation of the incident wave in the negative z direction. At Fig. 4 it corresponds to placing the TF/SF surface after the structure and interchange between transmittance and reflectance detectors. If the structure possesses a certain symmetry, elements $M^{--}_{\mathbf{g}j,\mathbf{g}'j'}$, $M^{+-}_{\mathbf{g}j,\mathbf{g}'j'}$ can be expressed through $M^{++}_{\mathbf{g}j,\mathbf{g}'j'}$, $M^{-+}_{\mathbf{g}j,\mathbf{g}'j'}$. For example, if structure is symmetrical under 180° rotations around the x axis, $M^{-\pm}_{g_x,g_y,j,g'_x,g'_y,j'} = M^{+\mp}_{-g_x,g_y,j,-g'_x,g'_y,j'}$. Other types of symmetry can result in further reduction of number of independent transfer matrix elements.

Note that the transfer-matrix elements express a relation between the transmitted (reflected) and incident magnetic field in a similar way as for the electric one (42), (43):

$$[H_{\text{tr}}]^+_{\mathbf{g}j} = M^{++}_{\mathbf{g}j,\mathbf{g}'j'} [H_{\text{in}}]^+_{\mathbf{g}'j'}. \tag{51}$$

$$[H_{\text{rf}}]^-_{\mathbf{g}j} = M^{-+}_{\mathbf{g}j,\mathbf{g}'j'} [H_{\text{in}}]^+_{\mathbf{g}'j'}. \tag{52}$$

As we checked numerically, calculation of the transfer matrix elements using the relation between magnetic fields can produce more accurate results in the case of p polarization. In this case, the $\mathbf{H}$ field is directed along the s-polarization vector with a zero z component, while $\mathbf{E}$ is directed along the p-polarization vector with nonzero x, y, and z components. Thus, in this case, the $\mathbf{H}$ field is better aligned with the FDTD rectangular mesh.

IV. TESTS

We implemented the transfer-matrix technique as a part of the Electromagnetic Template Library, which is available online [26]. To test our technique we calculate the transmittance from opal photonic crystal slab formed by conductive ($\varepsilon = 1.5, \sigma = 0.5$) spheres of the radius $R = 0.3$. The spheres are packed in a cubic lattice with period $a = 1$. We consider four-layered and 32-layered photonic crystal slabs (each layer is square lattice of spheres). We choose the mesh step $\Delta r = 0.05$. Note that simulation of opal photonic crystals requires a special concern since their spherical elements should be adequately discretized on the rectangular FDTD mesh. This is done with the help of a subpixel smoothing method, which significantly improves the FDTD accuracy for arbitrarily shaped scatterers [27]. We use a variation of this method, which is applicable for conductive and dispersive media that can be specified by arbitrary number of Drude, Lorentz [18], and modified Lorentz terms [28]. To reduce undesired numerical reflection from the PMLs we use the additional back absorbing layers technique [24], as discussed in the previous section.

To build the transfer matrix we perform simulations for the three incident vectors $\mathbf{g}'$: (0,0), (1,0), (1,1) and both polarizations. Using results of simulations with the structure and without it (vacuum), we calculate the transfer matrix according to the procedure described in section III. Taking into account the symmetry of the square lattice, we find the transfer matrix elements for nine vectors $\mathbf{g}' = m_1\mathbf{b}_1 + m_2\mathbf{b}_2$, where $m_i = -1,0,1$, $|m_1| + |m_2| \leqslant 1$, both polarizations and directions (forward and backward) of incident wave. Applying the multiplication procedure described in Sec. II, we obtain 18×18 transfer matrix for an n-layered photonic crystal slab. Transmittance spectra can be calculated using (27). The obtained 18×18 transfer matrix allows to obtain accurate results for the frequency range $0 \leqslant f \leqslant 2$.

At Fig. 5 we present the calculated transmittance for 32-layered photonic crystal. We compare it with the results obtained using direct FDTD simulation and the on-shell layer multiple scattering (LMS) method [14,15]. Results obtained by these three different methods are in good agreement with each other. The accuracy of LMS results decreases at low frequencies due to the poor convergence of the Chebyshev series for spherical Bessel functions. Note that there is unphysical transmittance peak at the frequency $f \approx 1$ calculated by our hybrid technique. At this frequency one of

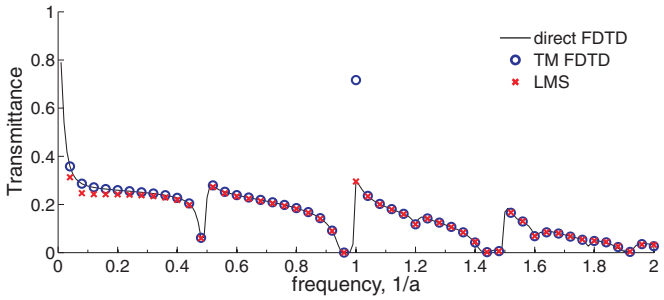

FIG. 5. (Color online) Transmittance spectra for 32-layered photonic crystal slab formed by conducting ($\varepsilon = 1.5$, $\sigma = 0.5$) spheres of the radius $R = 0.3$. Spheres are packed in cubic lattice with period $a = 1$. Results are obtained using FDTD, hybrid transfer matrix FDTD method, and on-shell layer multiple scattering (LMS) method.

the allowed nonevanescent scattered wave directions is almost parallel to the plane of the photonic crystal slab. This wave is poorly absorbed by PML that negatively affects accuracy of the transfer-matrix calculation.

In order to illustrate the importance of taking into account the matrix elements corresponding to the evanescent waves, we recalculated the transmittance using a simplified transfer matrix, where all elements corresponding to the evanescent waves $(k_z)^2 < 0$ were set to zero (which is not correct). The calculation was performed for 32- and four-layered photonic crystals. One can see that the accuracy of the obtained results deteriorates for frequencies $f \approx 1, \sqrt{2}$ (Fig. 6). At these frequencies the attenuation factor for some evanescent waves approaches zero. These evanescent waves have more chance to be rescattered into propagating waves inside the layer and contribute to the wave propagation through the entire structure.

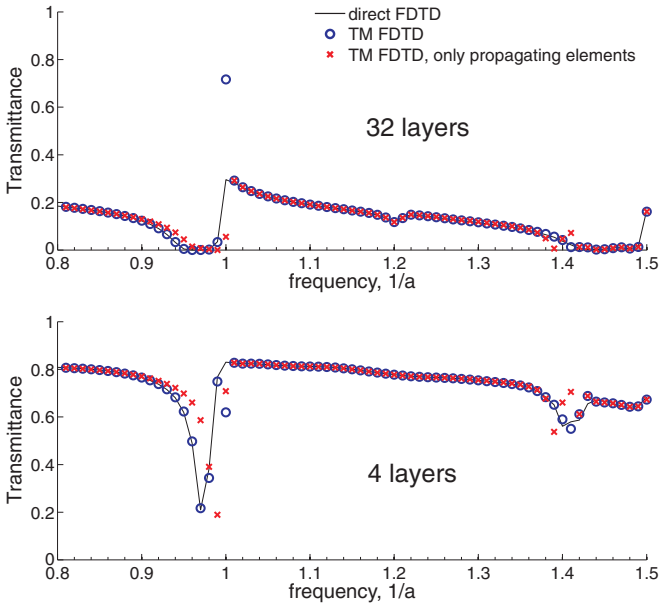

FIG. 6. (Color online) Transmittance spectra for 32-layered (top) and four-layered (bottom) photonic crystal formed by conducting ($\varepsilon = 1.5, \sigma = 0.5$) spheres of the radius $R = 0.3$. Spheres are packed in cubic lattice with period $a = 1$. Ignoring transfer-matrix elements corresponding to evanescent waves results in low accuracy for frequencies $f \approx 1, \sqrt{2}$.

Therefore ignoring the transfer-matrix elements corresponding to evanescent waves leads to a decrease in accuracy.

Our hybrid technique works faster compared to a direct FDTD calculation for a 32-layered slab, while for a four-layered slab direct FDTD simulation is still more efficient. Note that the hybrid technique can be preferable for modeling of purely dielectric (nonabsorbing) multilayered slabs. Light entering such a structure can spend a long time there before being finally transmitted (reflected) [24], which leads to increased simulation times in the standard FDTD. At the same time, the calculation of transfer matrix requires the simulation of a single layer only and can be done relatively fast.

V. DISCUSSION

The presented method can be successfully used for calculation of photonic band structure. Typically, band structure is calculated using the plane wave expansion (PWE) method, which relies on expanding the eigenmodes in a series of plane waves [3]. This leads to a finite matrix eigenproblem, which can be solved using the standard linear algebra or certain iterative techniques [29]. However, PWE becomes inefficient for photonic crystals formed by sharp geometrical features, since the number of plane waves in expansion could be very large [30]. Frequency-dependent materials are another obstacle for standard PWE formulation, since in this case the eigenvalue problem is nonlinear and difficult to solve. This problem can be simplified by using the basis function of dielectric backbone structure [31], introduction of auxiliary fields [32] (similar approach was recently developed for weakly nonlinear materials [33]), or applying Dirichlet-to-Neumann map [34,35]. Alternatively, the band structure can also be calculated by regarding frequency ω and $\mathbf{q}_\parallel$ as parameters and relating the eigenvalue to a component of the Bloch wave vector $\mathbf{q}_z$ [36–38]. This leads to a linear eigenvalue problem even for dispersive materials. This eigenproblem can be defined using transfer-matrix formalism [14,15]. Thus, calculation of band structure can be done using the transfer matrices for the entire set of wave vectors inside the irreducible part of the Brillouin zone. A detailed way to calculate the transfer matrix using FDTD for $\mathbf{q}_\parallel = 0$ is described in Sec. III, while calculation for nonzero $\mathbf{q}_\parallel$ is a trivial extension, which requires applying Bloch-periodic boundary conditions (29). The hybrid FDTD transfer-matrix technique is a good alternative to common way to calculate eigenmodes in FDTD where eigenmodes are extracted from peaks in spectral response to some excitation pulse [39–41].

Our method can be combined with the existing FDTD methods for simulation of periodic structures at the oblique incidence [42–50]. For example, the transfer matrix may be calculated as described above for an obliquely incident plane wave, which can be simulated using an iterative technique [42,43]. In this case, the incident angle is fixed for all frequencies. Therefore $\mathbf{q}_\parallel$ is different for each frequency. It modifies the definition of the incident wave (37), but the way to calculate the transfer matrix remains the same.

Finally, while the above method is derived for a plane incident wave (with a given $\mathbf{k}_\parallel$), it can be extended for the case of an arbitrary source wave (i.e., a point dipole source). In this case, a proper decomposition of the source term in

propagating and evanescent waves should be used instead of (6). This decomposition may require the summation of different $\mathbf{k}_\parallel$ (integration over the Brillouin zone), which is the case when the typical wavelength of the incident source wave is smaller or comparable to the period of the structure. This approach can be very useful in modeling of light extraction from patterned OLEDs [20,51,52]. In such setup, a dipole source is positioned inside a multilayered OLED stack in a close proximity to periodically patterned surfaces. In the standard FDTD, the computational domain cannot be reduced to a single unit cell of the structure due to the local nature of the dipole source. Therefore a sufficiently large domain bordered with the PML should be used in the calculation in order to avoid truncation errors, which is very time consuming. However, the hybrid technique described in this paper allows using only a single unit cell and performing a set of calculations for each term in the source decomposition, which appears to be much more efficient than the standard approach. Subsequently the results of all calculations are summed up to obtain the result for the dipole in the periodic structure.

VI. CONCLUSION

In this paper, we presented a detailed description of the hybrid method for calculation of transfer matrices of periodic structures with the FDTD method, as well as its efficient implementation. The transfer matrix for a single-layered periodic structure can be extracted from series of FDTD simulations. The transfer matrix of a multilayered structure is obtained as a recursive product of transfer matrices of the constituent single layers. Our approach combines advantages of both FDTD and transfer-matrix methods. First, it borrows the capability of FDTD to handle scatterers with an arbitrary geometry, which cannot be easily done in transfer-matrix methods. Second, it keeps the key feature of transfer-matrix methods, where one only needs to calculate the transfer matrix of the single layer once, while it can be used later for calculation of transfer matrices of multilayered structures composed by arbitrary sequence of single layers. This makes our method faster than the standard FDTD for calculation of optical properties of multilayered structures (thick photonic slabs).

We applied the method to the calculation of reflectance and transmittance spectra of multilayered photonic crystals and particularly discussed the role of evanescent waves in the wave propagation through the periodic structure. The issue of properly incorporating the evanescent waves into the FDTD calculation is also addressed.

Finally, we discuss the application of our method for calculation of photonic band structures, simulation of oblique incidence, and point sources inside a periodical environment.

ACKNOWLEDGMENTS

The work was partially supported by The Ministry of Science and Education of Russia under the Contract No. 16.523.11.3004.

[1] S. John, Phys. Rev. Lett. **58**, 2486 (1987).
[2] E. Yablonovitch, Phys. Rev. Lett. **58**, 2059 (1987).
[3] K. Sakoda, *Optical Properties of Photonic Crystals*, 2nd ed. (Springer-Verlag, Berlin, 2004).
[4] E. Istrate and E. H. Sargent, Rev. Mod. Phys. **78**, 455 (2006).
[5] J. B. Pendry and A. MacKinnon, Phys. Rev. Lett. **69**, 2772 (1992).
[6] J. B. Pendry, J. Phys.: Condens. Matter **8**, 1085 (1996).
[7] P. M. Bell, J. B. Pendry, L. M. Moreno, and A. J. Ward, Comp. Phys. Comm. **85**, 306 (1995).
[8] I. El-Kady, M. M. Sigalas, R. Biswas, K. M. Ho, and C. M. Soukoulis, Phys. Rev. B **62**, 15299 (2000).
[9] L. Li, J. Opt. Soc. Am. A **13**, 1024 (1996).
[10] Z.-Y. Li and L.-L. Lin, Phys. Rev. E **67**, 046607 (2003).
[11] Z.-Y. Li, Sci. Technol. Adv. Mater. **6**, 837 (2005).
[12] Z.-Y. Li and K.-M. Ho, Phys. Rev. B **68**, 155101 (2003).
[13] N. Stefanou, V. Karathanos, and A. Modinos, J. Phys.: Condens. Matter **4**, 7389 (1992).
[14] N. Stefanou, V. Yannopapas, and A. Modinos, Comput. Phys. Commun. **113**, 49 (1998).
[15] N. Stefanou, V. Yannopapas, and A. Modinos, Comput. Phys. Commun. **132**, 189 (2000).
[16] V. Yannopapas, N. Stefanou, and A. Modinos, Phys. Rev. Lett. **86**, 4811 (2001).
[17] G. Gantzounis and N. Stefanou, Phys. Rev. B **73**, 035115 (2006).
[18] A. Taflove and S. H. Hagness, *Computational Electrodynamics: The Finite Difference Time-Domain Method* (Artech House, Boston, 2005).
[19] S. Belousov, M. Bogdanova, A. Deinega, S. Eyderman, I. Valuev, Yu. Lozovik, I. Polischuk, B. Potapkin, B. Ramamurthi, T. Deng, and V. Midha, Phys. Rev. B **86**, 174201 (2012).
[20] Y.-J. Lee, S.-H. Kim, J. Huh, G.-H. Kim, Y.-H. Lee, S.-H. Cho, Y.-C. Kim, and Y. R. Do, Appl. Phys. Lett. **82**, 3779 (2003).
[21] A. F. Koenderink, M. Kafesaki, and C. M. Soukoulis, J. Opt. Soc. Am. B **23**, 1196 (2006).
[22] A. Deinega, S. Belousov, and I. Valuev, Opt. Lett. **34**, 860 (2009).
[23] A. Aminian and Y. Rahmat-Samii, IEEE Trans. Antennas and Propagation **54**, 1818 (2006).
[24] *Fast Fourier Transforms*, edited by C. Sidney Burrus (Rice University, Houston, 2009).
[25] A. Deinega and I. Valuev, Comp. Phys. Comm. **182**, 149 (2011).
[26] Electromagnetic Template Library (EMTL), Kintech Lab Ltd, http://fdtd.kintechlab.com.
[27] A. Deinega and I. Valuev, Opt. Lett. **32**, 3429 (2007).
[28] A. Deinega and S. John, Opt. Lett. **37**, 112 (2012).
[29] S. G. Johnson and J. D. Joannopoulos, Opt. Express **8**, 173 (2001).
[30] H. S. Sozuer, J. W. Haus, and R. Inguva, Phys. Rev. B **45**, 13962 (1992).
[31] G. Alagappan and A. Deinega, PIER B **52**, 1 (2013).
[32] A. Raman and S. Fan, Phys. Rev. Lett. **104**, 087401 (2010).
[33] Y. Zeng, D. A. R. Dalvit, J. O'Hara, and S. A. Trugman, Phys. Rev. B **85**, 125107 (2012).
[34] J. Yuan and Y. Y. Lu, JOSA A **23**, 3217 (2006).
[35] J. Yuan, Y. Y. Lu, and X. Antoine, J. Comp. Phys. **227**, 4617 (2008).

[36] Y.-C. Hsue and T.-J. Yang, Phys. Rev. E **70**, 016706 (2004).
[37] S. Shi, C. Chen, and D. W. Prather, Appl. Phys. Lett. **86**, 043104 (2005).
[38] A. A. Sedghi, M. Kalafi, A. Soltani Vala, and B. Rezaei, Opt. Commun. **283**, 2356 (2010).
[39] C. T. Chan, Q. L. Yu, and K. M. Ho, Phys. Rev. B **51**, 16635 (1995).
[40] K. Sakoda, N. Kawai, T. Ito, A. Chutinan, S. Noda, T. Mitsuyu, and K. Hirao, Phys. Rev. B **64**, 045116 (2001).
[41] G. A. Stark, M. Mishrikey, F. Robin, H. Jaeckel, C. Hafner, R. Vahldieck, and D. Erni, Int. J. Numer. Model. **22**, 201 (2009).
[42] I. Valuev, A. Deinega, and S. Belousov, Opt. Lett. **33**, 1491 (2008).
[43] I. Valuev, A. Deinega, and S. Belousov, Comp. Phys. Comm. (to be published).
[44] G. Zheng, A. A. Kishk, A. W. Glisson, and A. B. Yakovlev, Progress In Electromagnetics Research **59**, 85 (2006).
[45] S. M. Amjadi and M. Soleimani, Progress Electromagn. Res. B **43**, 271281 (2008).
[46] A. Belkhir, O. Arar, S. S. Benabbes, O. Lamrous, and F. I. Baida, Phys. Rev. E **81**, 046705 (2010).
[47] A. Shahmansouri and B. Rashidian, JOSA B **28**, 2690 (2011).
[48] J. Frances, J. Tervo, and A. Marquez, JOSA B **30**, 1711 (2013).
[49] F. Yang, J. Chen, R. Qiang, and A. Elsherbeni, Radio Science **42**, RS4004 (2007).
[50] Y.-J. Zhou, X. Zhou, T.-J. Cui, R. Qiang, and J. Chen, PIER M **17**, 101 (2011).
[51] Y.-J. Lee, S.-H. Kim, G.-H. Kim, Y.-H. Lee, S.-H. Cho, Y.-W. Song, Y.-C. Kim, and Y. R. Do, Opt. Exp. **13**, 5864 (2005).
[52] A. O. Altun, S. Jeon, J. Shim, J.-H. Jeong, D.-G. Choi, K.-D. Kim, J.-H. Choi, S.-W. Lee, E.-S. Lee, H.-D. Park, J. R. Youn, J.-J. Kim, Y.-H. Lee, and J.-W. Kang, Org. Electron. **11**, 711 (2010).